Design criteria for optimally tuned vibro-impact nonlinear energy sink

Donghai Qiu, Sébastien Seguy, Manuel Paredes

Design criteria for optimally tuned vibro-impact nonlinear energy sink

D. Qiu[a,*], S. Seguy[b], M. Paredes[b]

[a]*Suzhou Institute of Biomedical Engineering and Technology, Chinese Academy of Sciences, 88 Keling Road, 215163, Suzhou, China*
[b]*Institut Clément Ader (ICA), CNRS-INSA-ISAE-Mines Albi-UPS, Université de Toulouse, 3 rue Caroline Aigle, 31400, Toulouse, France*

Abstract

This paper proposes the design criteria for optimally tuned Vibro-Impact (VI) Nonlinear Energy Sink (NES) to control vibration under periodic and transient excitation. Firstly, a generalized dimensionless model of a two degrees of freedom (DOF) system comprising a harmonically excited linear oscillator (LO) strongly coupled to a VI NES is investigated. Bifurcation analysis and efficiency of Targeted Energy Transfer (TET) around the Slow Invariant Manifold (SIM) are studied with the variation of clearance. As a result, the optimal clearances for periodic and transient excitation are calculated from two transition points of the SIM, respectively. Then the procedure is extended to the case of multiple VI NESs in parallel with the LO. Two principles of additivity and separate activities of VI NESs are verified theoretically. Finally, experiments involving the whole system embedded on an electrodynamic shaker are performed. The results show that the design criteria can not only predict the efficient TET at resonance frequency, but can also achieve an optimal performance in a range of frequencies. Furthermore, the criteria can be straightforward for the application of multiple VI NESs, so as to make VI NESs work robustly under different types of excitation.

Keywords: Vibro-impact, Nonlinear energy sink, Optimal design, Activation energy, Targeted energy transfer, Passive vibration control

*Corresponding author

Email addresses: qiudh@sibet.ac.cn (D. Qiu), sebastien.seguy@insa-toulouse.fr (S. Seguy), manuel.paredes@insa-toulouse.fr (M. Paredes)

1. Introduction

Vibrating systems with clearance between the moving parts, such as linkages, gear trains, pinned connections and joints, are frequently encountered in engineering fields. Impacts occur when the vibration amplitudes of some parts are greater than the clearance, leading to high energy being transferred and dissipated in a transient manner. This phenomenon is attractive for vibration control, and a corresponding device, called an impact damper, was developed in 1945 [1]. Over the past decades, impact damper and its dynamics as a typical vibro-impact system have been extensively studied [2, 3, 4] and it has been demonstrated that in a range of frequencies, an impact damper can perform better efficiency than a classical damper. With this advantage, various applications of impact damper can be found in turbine blades, machine tools and tall flexible structures [5, 6, 7].

Recently, impact damper has been re-examined from the viewpoint of Targeted Energy Transfer (TET) [8, 9], and is then referred to as Vibro-Impact (VI) Nonlinear Energy Sink (NES) [10, 11, 12]. In the present work, the mechanism of TET is revealed by analytical study of underlying Hamiltonian system [13] and it is observed that some special orbits in the frequency-energy plot are responsible for the irreversible energy transfer from a primary system to an attached VI NES. Inspired by the study of TET, a method of multiple scales originally used for NES with cubic nonlinearity has been improved to explain the transient TET process for a vibrating system with a VI NES [14]. Consequently, a Slow Invariant Manifold (SIM) describing all possible fixed points and possible variation routes is obtained [15, 16].

As far as design criteria of VI NES, there are two main research themes, namely activation characteristic and parameter optimization. With respect to the activation, it is experimentally found that VI NES with a fixed outside excitation is activated in a fixed interval of clearance, and also a VI NES with a fixed clearance is activated in a fixed interval of displacement amplitude of a linear primary system [17]. Theoretically, the above two describe the same thing, namely VI NES as a vibration absorber will only be effective in a range of some parameter, no matter this parameter is displacement amplitude of the primary system, or amplitude of the excitation, or energy. In [18], the activation characteristic of VI NES generalized from linear systems to nonlinear systems is studied. It shows that the activation characteristic is independent of frequency, so the design of a VI NES for a nonlinear system can be simplified to the optimal design of a linear system. In [19], this kind of design characteristic is explored for a nonlinear vibration absorber, but in a general way. The basic philosophy of this design is reflected in the

relation of activation energy and clearance of VI NES.

In terms of parameter optimization, it is found that the regime with two impacts per cycle plays an optimal role, no matter in permanent form or intermittent form [20]. Based on this idea, a design procedure is proposed, which is similar in essence to the case of a NES with cubic nonlinearity [21]. For periodic excitation, the objective is to tune the response at the boundary between two symmetrical impacts per cycle and Strongly Modulated Response (SMR). For transient excitation, the target is to make the free response start at the regime with two impacts per cycle and ensure that its duration is as long as possible. In [22], this optimal mechanism is extended to a linear system coupled with two VI NES in parallel. However, the optimal values of clearance are obtained by trial and errors in [20, 22]. If the primary system and the excitation are changed, the clearance will no longer be optimal. Thus, ways of ensuring the optimal response by precise analytical calculation for the clearance need to be further studied.

Unlike NES with cubic nonlinearity, VI NES is capable of passively absorbing and dissipating significant portions of the energy of a primary system, at sufficiently fast time scales, which render it suitable for applications like seismic mitigation [13]. However, for both the linear and nonlinear system, the activation of VI NES is limited to a range of excitation. This means that a fixed clearance will only be effective in a given range of displacement amplitudes of a primary system. Using multiple VI NESs is an alternative way to improve the robustness and the feasibility of this approach is proved in the case of multiple NESs with cubic nonlinearity [23, 24]. In [22], two VI NESs, one with a medium clearance and one with a small clearance, are proposed to be optimal for a given excitation, and experimental results demonstrate their efficiency. Yet, how to adapt the design from a single VI NES to multiple VI NESs is still not clear, neither is the corresponding calculation.

Therefore, the first objective of this paper is to provide a precise analytical calculation of clearance for a single VI NES, and the second is to establish the optimal design relation for passing from a single VI NES to multiple VI NESs, so as to obtain VI NESs that work robustly under different systems and different types of excitation. The paper is organized as follows. Section 2 and Section 3 present the asymptotic analysis of a single VI-NES and the optimal design criteria to tune the clearance for periodic and transient excitation. In Section 4, targeted energy transfer of multiple VI NESs in parallel is studied. In Section 5, details of the experiments performed on the whole system embedded on an electrodynamic shaker are presented. Finally, some conclusions are proposed.

2. Asymptotic analysis of a single VI-NES

2.1. Dynamic modelling

The dynamic modelling presented here is based on [18] and [25]. The system of a harmonically excited linear oscillator (LO) attached to a VI NES is illustrated in Fig. 1. The objective here is to apply the asymptotic method used in the above papers to deduce the generalized dimensionless model, so as to obtain the optimal design criteria for a VI NES intended for any targeted primary system.

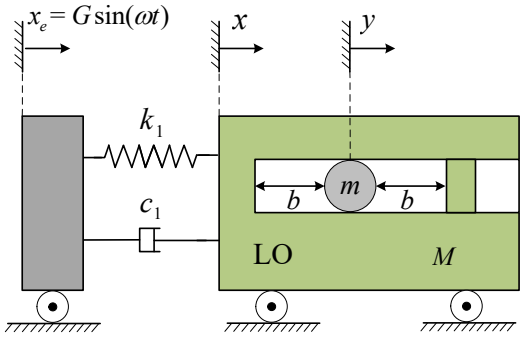

Figure 1: Schematic of the dynamic system: a harmonically excited LO coupled with a VI NES

The system is excited by the base, and the equations of motion between impacts are described as follows:

$$\begin{aligned} &M\ddot{x} + c_1\dot{x} + k_1 x = k_1 x_e + c_1 \dot{x_e} \\ &m\ddot{y} = 0, \qquad \forall |x-y| < b \end{aligned} \tag{1}$$

where x, M, c_1 and k_1 are the displacement, mass, damping and stiffness of the LO, respectively. y and m are the displacement and mass of VI NES. b represents the clearance, which can be adjusted by the length of cavity. The imposed harmonic displacement x_e is expressed as:

$$x_e = G\cos(\omega t) \tag{2}$$

When $|x-y| = b$, an impact occurs. The state of the model after impact is obtained by using the simplified shock theory:

$$\begin{aligned} &x^+ = x^-, \quad y^+ = y^- \\ &\dot{x}^+ - \dot{y}^+ = -r\left(\dot{x}^- - \dot{y}^-\right) \end{aligned} \tag{3}$$

where r is the restitution coefficient and the superscripts $+$ and $-$ denote time immediately after and before impact. By virtue of the condition of total momentum conservation, it gives:

$$M\dot{x}^{+} + m\dot{y}^{+} = M\dot{x}^{-} + m\dot{y}^{-} \tag{4}$$

Then the following changes of variables are introduced:

$$\varepsilon = \frac{m}{M}, \quad {\omega_0}^2 = \frac{k_1}{M}, \quad \tau = \omega_0 t, \quad \lambda = \frac{c_1}{m\omega_0}, \quad \Omega = \frac{\omega}{\omega_0}, \quad F = \frac{G}{\varepsilon b} \tag{5}$$

The variables of the displacements are dimensioned by:

$$x = Xb, \quad y = Yb \tag{6}$$

After rescaling, the system of equation (1) can be reduced to the dimensionless form:

$$\begin{aligned} &\ddot{X} + \varepsilon\lambda\dot{X} + X = \varepsilon F \sin\Omega\tau + \varepsilon^2\lambda F\Omega\cos\Omega\tau \\ &\varepsilon\ddot{Y} = 0, \qquad \forall |X-Y| < 1 \end{aligned} \tag{7}$$

When $|X-Y| = 1$, an impact occurs, and the equations (3) and (4) are written as:

$$\begin{aligned} &X^{+} = X^{-}, \quad Y^{+} = Y^{-} \\ &\dot{X}^{+} + \varepsilon\dot{Y}^{+} = \dot{X}^{-} + \varepsilon\dot{Y}^{-} \\ &\dot{X}^{+} - \dot{Y}^{+} = -r\left(\dot{X}^{-} - \dot{Y}^{-}\right), \quad \text{for } |X-Y| = 1 \end{aligned} \tag{8}$$

Two new variables representing the displacement of the center of mass and the internal displacement of the VI NES are introduced (both of them are dimensionless):

$$V = X + \varepsilon Y, \quad W = X - Y \tag{9}$$

Substituting Eq. (9) into Eqs. (8) and (7), the equation between impacts in barycentric coordinates becomes:

$$\begin{aligned} &\ddot{V} + \varepsilon\lambda\frac{\dot{V} + \varepsilon\dot{W}}{1+\varepsilon} + \frac{V + \varepsilon W}{1+\varepsilon} = \varepsilon F \sin\Omega\tau \\ &\ddot{W} + \varepsilon\lambda\frac{\dot{V} + \varepsilon\dot{W}}{1+\varepsilon} + \frac{V + \varepsilon W}{1+\varepsilon} = \varepsilon F \sin\Omega\tau, \quad \forall |W| < 1 \end{aligned} \tag{10}$$

where the term containing ε^2 is very small and can be neglected. The impact condition (8) can be rewritten as:

$$\begin{aligned} &V^+ = V^-, \quad W^+ = W^-, \\ &\dot{V}^+ = \dot{V}^-, \quad \dot{W}^+ = -r\dot{W}^-, \quad \text{for } |W| = 1 \end{aligned} \tag{11}$$

Then multiple scales are introduced in the following forms:

$$\begin{aligned} &V(\tau;\varepsilon) = V_0(\tau_0,\tau_1,\ldots) + \varepsilon V_1(\tau_0,\tau_1,\ldots) + \ldots \\ &W(\tau;\varepsilon) = W_0(\tau_0,\tau_1,\ldots) + \varepsilon W_1(\tau_0,\tau_1,\ldots) + \ldots \\ &\tau_k = \varepsilon^k \tau, \quad k = 0,1,\ldots \end{aligned} \tag{12}$$

The system is studied in the vicinity of the 1:1 resonance, where both the LO and the VI NES execute time periodic oscillations with identical frequency. Thus, a detuning parameter σ representing the nearness of the forcing frequency Ω to the reduced natural frequency of the LO is introduced:

$$\Omega = 1 + \varepsilon\sigma \tag{13}$$

Substituting Eqs. (12) and (13) into Eqs. (10) and (11), then equating coefficients of like power of ε gives:

Order ε^0:

$$\begin{aligned} &D_0^2 V_0 + V_0 = 0 \\ &D_0^2 W_0 + V_0 = 0, \quad \forall |W_0| < 1 \end{aligned} \tag{14}$$

$$\begin{aligned} &V_0^+ = V_0^-, \quad W_0^+ = W_0^-, \quad \text{for} |W_0| = 1 \\ &D_0 V_0^+ = D_0 V_0^-, \quad D_0 W_0^+ = -r D_0 W_0^- \end{aligned} \tag{15}$$

Order ε^1:

$$\begin{aligned} &D_0^2 V_1 + V_1 = -2D_0 D_1 V_0 - \lambda D_0 V_0 - W_0 + V_0 + F\sin(\tau_0 + \sigma\tau_1) \\ &D_0^2 W_1 + V_1 = -2D_0 D_1 V_0 - \lambda D_0 V_0 - W_0 + V_0 + F\sin(\tau_0 + \sigma\tau_1) \\ &\forall |W_0| < 1 \end{aligned} \tag{16}$$

where D_0 represents partial derivative with respect to time τ_0. From the first equation of system (14), the solution of V_0 (in slow time scale) can be deduced as follows:

$$V_0 = A(\tau_1)\sin(\tau_0 + \theta(\tau_1)) \tag{17}$$

where $A(\tau_1)$ and $\theta(\tau_1)$ represent the amplitude and phase of the LO, respectively. For W_0 (in slow time scale), Eqs. (14) and (15) represent a harmonically forced impact oscillator with symmetric barrier. Under the assumption of $1:1$ resonance, its solution can be sought in the following form:

$$W_0 = A(\tau_1)\sin(\tau_0 + \theta(\tau_1)) + \frac{2}{\pi}C(\tau_1)\Pi(\tau_0 + \eta(\tau_1)) \tag{18}$$

where $C(\tau_1)$ and $\eta(\tau_1)$ represent the amplitude and phase of VI NES, respectively. $\Pi(z)$ is a non-smooth saw tooth function [26]. Its folded function is expressed as follows:

$$\Pi(z) = \arcsin(\sin z), \quad M(z) = \frac{d\Pi}{dz} = sgn(\cos z) \tag{19}$$

As can be observed from Eqs. (18) and (19), impact occurs at $\tau_0 = \pi/2 - \eta + j\pi$ with $j = 0, 1, 2, \ldots$ Substituting the above equations in the impact condition Eq. (15) yields:

$$cos(\eta - \theta) = \frac{1-C}{A}, \quad sin(\eta - \theta) = \frac{2C\Gamma}{\pi A} \tag{20}$$

where $\Gamma = (1-r)/(1+r)$. By combining the above two equations with trigonometric identity, the expression for a Slow Invariant Manifold (SIM) is obtained:

$$A^2 = (1-C)^2 + \frac{4C^2\Gamma^2}{\pi^2} \tag{21}$$

2.2. Analytical treatment of Slow Invariant Manifold (SIM)

An illustration of the SIM is presented in Fig. 2. Unlike for a cubic NES, the SIM has a topological structure composed of two branches. It can be observed that the left branch is unstable and only a part of the right branch is stable (between the points T_1 and T_2). The stability of the SIM can be evaluated by direct numerical integration of Eqs. (14) and (15).

Depending on the different positions of the fixed point in SIM [17], five types of response regimes are obtained: (1) chaos with no duration of two impacts per cycle, where no fixed point occurs and the energy is too low to activate the energy pumping; (2) chaos by intermittency, i.e., Strongly Modulated Response (SMR), with the fixed point located on the left unstable branch of the SIM; (3) two symmetric impacts per cycle, while the fixed point is located on the stable branch; (4) two asymmetric impacts per cycle, the fixed point starts to pass the transition

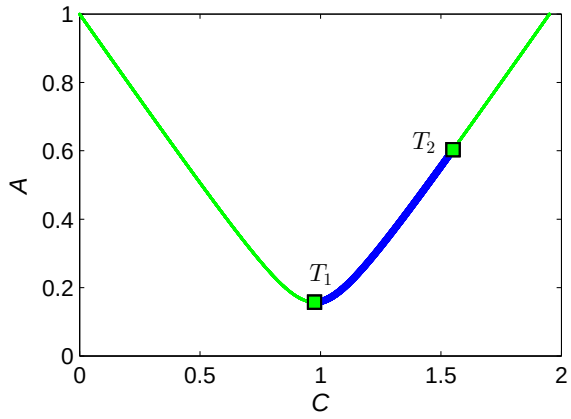

Figure 2: SIM of VI NES: on the stable branch in blue line and two unstable branches in green line with two transition point T_1 and T_2. $\varepsilon = 0.68\%$, $\lambda = 1.91$

point T_2 and stays on the right unstable branch; (5) chaos with an infinite number of impacts per cycle, i.e., the regime with more than two impacts per cycle, where the fixed point remains higher than in the above cases.

Knowing the variation mechanism of the response regimes, it would be interesting to investigate the efficiency of each regime and the corresponding threshold for periodic excitation, so as to guide the design of VI NES. In [20], it is demonstrated that the boundary between response with permanent two impacts per cycle and that with intermittent two impact cycle (SMR) is optimal, and the critical point is located at the extreme T_1 of the SIM. By setting the derivative of the right hand side of Eq. (21) to zero, its expression can be obtained as follows:

$$C_1 = \frac{\pi^2}{\pi^2 + 4\Gamma^2}, \quad A_1^2 = \frac{4\Gamma^2}{\pi^2 + 4\Gamma^2} \tag{22}$$

Here the value C_1 corresponds to the minimum amplitude of the LO, where 1:1 Targeted Energy Transfer (TET) is allowed. However, the precise analytical calculation of the cavity length (i.e., b) needed to ensure response at the critical point is still not clear and bifurcations of the system at the next order of approximation need to be analysed.

2.3. Bifurcation analysis

By introducing Eqs. (17) and (18) into the first equation of system (16) and eliminating the secular term, the asymptotic stability of the fixed points of the

stable branch with respect to time scale τ_1 is studied in the following form:

$$\begin{aligned} D_1 A &= \frac{F}{2}\sin(\sigma\tau_1-\theta)-\frac{4C}{\pi^2}\sin(\eta-\theta)-\frac{\lambda C}{2} \\ D_1\theta &= -\frac{F}{2A}\cos(\sigma\tau_1-\theta)+\frac{4}{\pi^2 A}B\cos(\eta-\theta) \end{aligned} \tag{23}$$

Substituting Eqs. (20) into Eq. (23) and introducing $\rho=\sigma\tau_1-\theta$, the expressions governing the evolution of the amplitude A and the phase ρ are obtained:

$$\frac{\partial A}{\partial\tau_1}=\frac{f_1(A,\rho)}{g(A)},\quad \frac{\partial\rho}{\partial\tau_1}=\frac{f_2(A,\rho)}{g(A)} \tag{24}$$

where

$$\begin{aligned} f_1 = {} & F\pi^3(1-A)\sin(\rho)+2FA\Gamma\pi^2\cos(\rho) \\ & -4\Gamma^2\pi A^2\lambda-16A^2\Gamma-\pi^3\lambda(A-1)^2 \end{aligned} \tag{25}$$

$$\begin{aligned} f_2 = {} & -2F\Gamma\pi\sin(\rho)-F\pi^2\cos(\rho)+8\Gamma^2 A\sigma \\ & +2\pi^2 A\sigma+2\Gamma\pi\lambda-2\pi^2\sigma+8A \end{aligned} \tag{26}$$

$$g=8\Gamma^2 A+2\pi^2 A-2\pi^2 \tag{27}$$

By equating the derivative of the right-hand side of Eq. (24) to zero, two kinds of fixed point are calculated. The first is referred to as an ordinary fixed point located on the stable branch of SIM, and it also satisfies the conditions $f_1=f_2=0$ and $g\neq 0$. The other corresponds to the folded singularity (i.e., T_1). In this case the derivative of Eq. (21) is related to Eq. (27), so it can be found that $g=0$. Based on this, the system $f_1=f_2=0$ will be discussed and is rewritten in the following matrix form:

$$\begin{bmatrix}\alpha_{11} & \alpha_{12}\\ \alpha_{21} & \alpha_{22}\end{bmatrix}\begin{bmatrix}\sin\rho\\ \cos\rho\end{bmatrix}=\begin{bmatrix}\beta_1\\ \beta_2\end{bmatrix} \tag{28}$$

where

$$\begin{cases} \alpha_{11}=F\pi^3(1-A),\quad \alpha_{12}=2FA\pi^2\Gamma, \\ \alpha_{21}=-2F\pi\Gamma,\quad \alpha_{22}=-F\pi^2 \\ \beta_1=4\Gamma^2\pi A^2\lambda+16A^2\Gamma+\pi^3\lambda(A-1)^2 \\ \beta_2=-8\Gamma^2 A\sigma-2\pi^2 A\sigma-2\Gamma\pi\lambda+2\pi^2\sigma-8A \end{cases} \tag{29}$$

By solving Eq. (28) for $\sin\rho$ and $\cos\rho$, ordinary fixed points can be obtained by assuming that the determinant does not vanish. For the folded singularity, it is observed that $\det(\alpha) = F^2\pi^3 g/2 = 0$, which means that, when f_2 and g are eliminated, the condition $f_1 = 0$ is automatically satisfied by Eq. (28). Thus the expression of $f_2 = 0$ can be studied in the following form:

$$\sqrt{\alpha_{21}^2 + \alpha_{22}^2} \cdot \cos(\rho - \delta) = \beta_2, \quad \delta = \arctan(\frac{\alpha_{21}}{\alpha_{22}}) \tag{30}$$

Then the phase ρ can be deduced as:

$$\rho = \arctan(\frac{\alpha_{21}}{\alpha_{22}}) + \arccos(\frac{\beta_2}{\sqrt{\alpha_{21}^2 + \alpha_{22}^2}}) \tag{31}$$

According to Eq. (31), the critical condition of the excitation amplitude for the folded singularity to exist is obtained:

$$\left| \frac{\beta_2}{\sqrt{\alpha_{21}^2 + \alpha_{22}^2}} \right| = 1 \tag{32}$$

Thus the threshold of the SMR is calculated as:

$$F_c = \frac{2(4A_I\Gamma^2\sigma + A_I\pi^2\sigma + \Gamma\pi\lambda - \pi^2\sigma + 4A_I)}{\pi\sqrt{4\Gamma^2 + \pi^2}} \tag{33}$$

Substituting Eq. (22) into Eq. (33), the threshold can be expressed in a convenient form:

$$F_c = \frac{2(4\Gamma^3\lambda + \Gamma\pi^2\lambda + 4\pi)}{(4\Gamma^2 + \pi^2)^{3/2}} \tag{34}$$

Here, it is noted that the variable F_c is a dimensionless variable of excitation, which is dependent only on the intrinsic properties of the LO and NES (i.e., the damping of the LO and the restitution coefficient).

3. Criteria for efficient targeted energy transfer

3.1. Optimal design criterion for SMR under periodic excitation

Based on the above analysis, the optimal design of VI NES is to make the target displacement amplitude of the LO locate at T_1 of the corresponding SIM

under periodic excitation. For this, the cavity length b is chosen as the design parameter, and the objective is to obtain its optimal value so as to produce efficient TET for different types of excitation. According to Eq. (5), the relation between the cavity length and the amplitude of excitation can be written as:

$$b = \frac{G}{\varepsilon F} \tag{35}$$

By introducing Eq. (34) into Eq. (35), the critical value of the cavity length is obtained as:

$$b_c = \frac{G\left(4\Gamma^2 + \pi^2\right)^{3/2}}{2\varepsilon(4\Gamma^3\lambda + \Gamma\pi^2\lambda + 4\pi)} \tag{36}$$

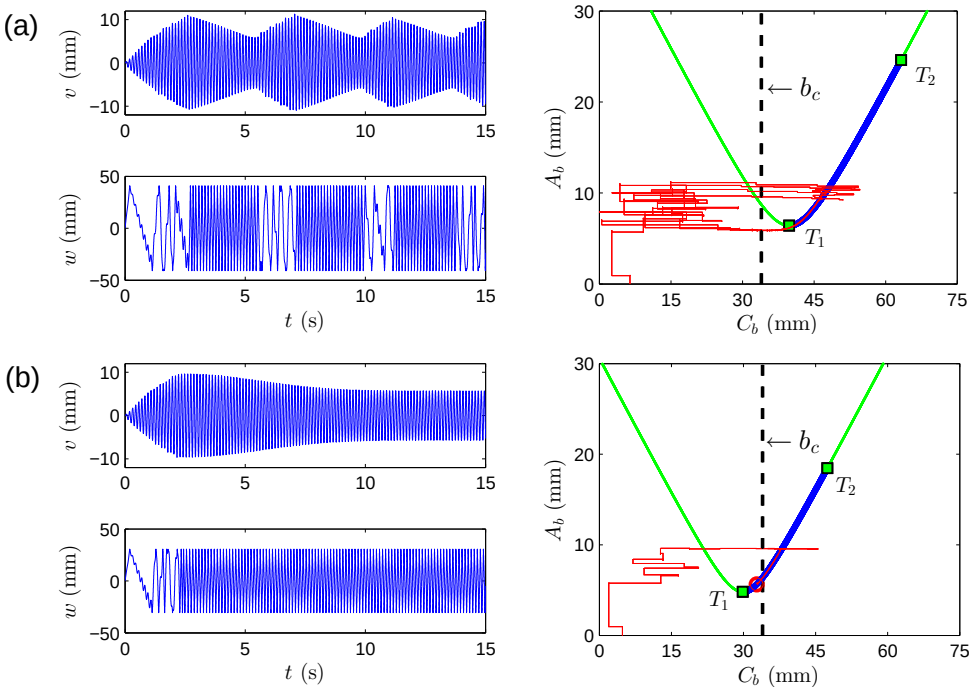

Figure 3: Time-displacement response of LO and VI NES, and the motion of the system projected into the SIM: (a) SMR with $b > b_c$; (b) steady state response with $b < b_c$.

To demonstrate the critical function of b_c, two response regimes with different cavity lengths are illustrated in Fig. 3. The time-displacement response of the LO

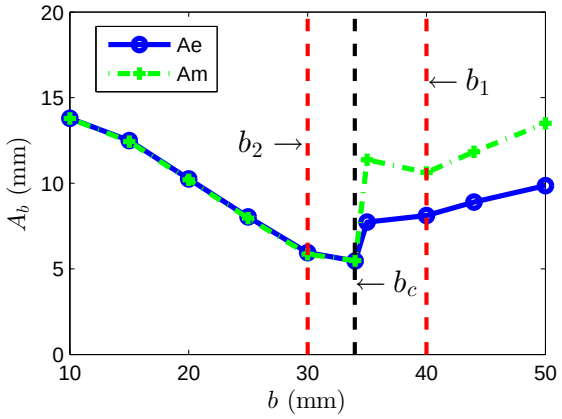

Figure 4: TET efficiency explained by the amplitude of LO with the variation of clearance b: A_e represents the mean amplitude and A_m the maximum amplitude.

and VI NES, and the projection of motion of the system into the SIM are presented in the first and second columns, respectively. As the cavity length is set to $b > b_c$, a strongly modulated response and its flow jump on the SIM are observed. In this case, the response acts through successive synchronization between the LO and the VI NES. When the VI NES is not synchronized, the amplitude of the LO grows. Under a certain circumstance, the VI NES enters into 1:1 resonance capture with the LO, making the amplitude of the LO decrease fast by successive impacts until it decays at the transition point T_1. As the cavity length is set as $b < b_c$, a steady state response with two symmetric impacts per cycle is observed. As can be seen, after a short transient motion, the flow is rapidly attracted to the red fixed point.

The variation law of TET efficiency with different lengths of cavity b under a fixed periodic excitation is presented in Fig. 4, where A_e and A_m represent the mean and the maximum amplitude of the LO, respectively. The two examples used above are illustrated by b_1 and b_2. As can be seen, when the clearance equals b_c, the amplitude of the LO is minimum. Thus the calculation of b_c can be used to provide the highest TET efficiency for the NES system.

3.2. Optimal design criterion for transient excitation

For the transient excitation, there does not exist SMR. The response regime transits continuously from one type to another with the decrease of the master energy. If the initial master energy is still set around the transition point T_1, the

NES system will rapidly pass the 1:1 resonance capture and enter the chaos with no duration of two impacts per cycle. In this case, the VI NES is only activated for a very short time, resulting in a low energy dissipation ratio being produced. In [20], it is demonstrated that the efficiency of TET should not only be high at the beginning but also last as long as possible. So in this paper, the transition point T_2 between the response with two symmetric and that with two asymmetric impacts per cycle is proposed for the position of the initial master energy. The analytical value of T_2 can be obtained from Fig. 2, with $A_2 = 0.6$. Based on this idea, the tuned parameter of the clearance b can be calculated in the following form:

$$b_t = \frac{x_m}{A_2}, \quad x_m = \sqrt{(x_0^2 + \frac{\dot{x}_0^2}{\omega_0^2})} \tag{37}$$

where x_m represents the initial master energy, x_0 and $\dot{x}_0$ represents the initial position and velocity of the LO, respectively.

To demonstrate the criterion, three cases with different clearances are calculated under the conditions: $G = 0$, $\dot{x}_0 = 0$ and $x_0 = 30$ mm. The tuned parameters are given in Table 1 and the optimal value b_t is obtained by Eq. (37), where x_1 and x_2 represent the amplitude of the LO at the transition points T_1 and T_2, $t_{x=15}$ and $t_{x=5}$ represent the time duration when the amplitude of the LO decreases to 15 mm and 5 mm, respectively.

Table 1: Three cases with different clearance under transient excitation

Tuned parameters					
case	b (mm)	x_1 (mm)	x_2 (mm)	$t_{x=15}$ (s)	$t_{x=5}$ (s)
$< b_t$	20	3.1	12	1.8	3.7
$= b_t$	50	7.8	30	1.3	2.6
$> b_t$	80	11.8	48.2	1	3.3

Transient responses of the first and second case with $b < b_t$ and $b = b_t$ are respectively presented in Fig. 5 (a) and (b). For the first case, four response regimes are observed during the whole process. A detailed view of these regimes can be found in Fig. 6. Firstly, the regime with three impacts per cycle is excited as shown in area a. Then the response of two asymmetric impacts per cycle appears consecutively as demonstrated in area b. When the amplitude of the system decreases to the transition point T_2, the flow starts to follow the fixed points on the

stable branch, which means that the response of two symmetric impacts per cycle with the 1:1 resonance capture is activated in area c. When the amplitude of the system decays to reach the transition point T_1, the system escapes from resonance capture, and the VI NES performs chaotic motion, as shown in area d.

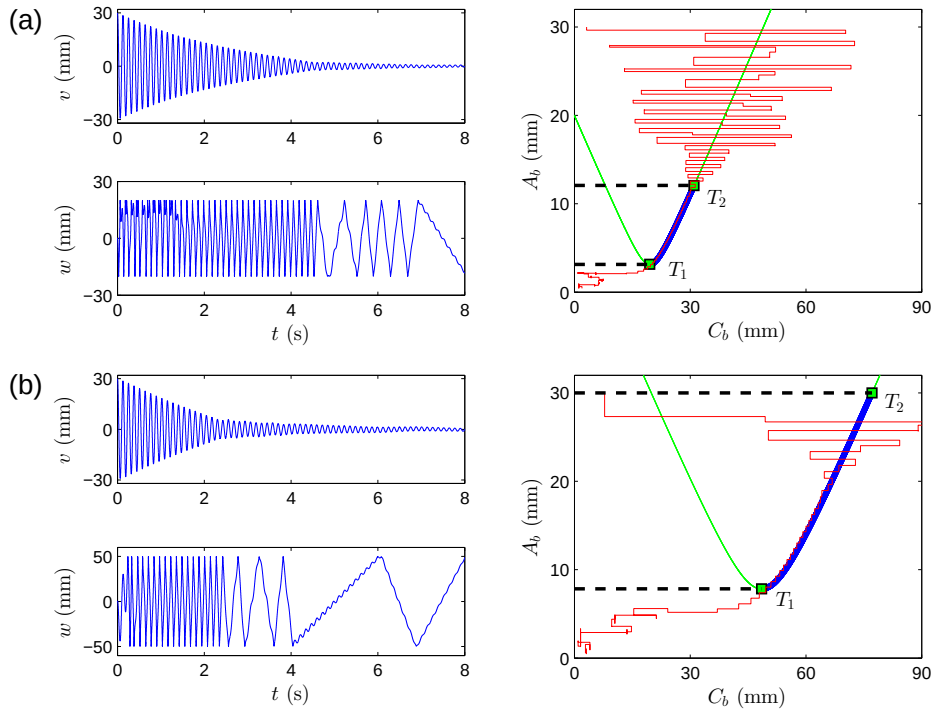

Figure 5: Time-displacement response of LO and VI NES, and the motion of the system projected into the SIM: (a) four response regimes with $b < b_t$; (b) two response regimes with $b = b_t$.

For the second case, as the cavity length is set as $b = b_t$, the master energy is directly decreased from T_2. Under a fast phase of nonlinear beating, the system enters the 1:1 resonance capture and the amplitude of the LO undergoes a higher decay ratio than in the first case. Meanwhile, with the increase of the clearance b, the SIM structure shifts to the upper right side, and the band of the stable branch largely increases. For the third case, the cavity length increases to $b > b_t$, making the initial master energy escape T_2 and approach T_1 more closely. As a result, its TET efficiency is large at the beginning period, as can be seen from the comparison of $t_{x=15}$ in Table 1. However, as the the amplitude of the LO decreases to 5 mm, the TET efficiency of this case becomes low and the second

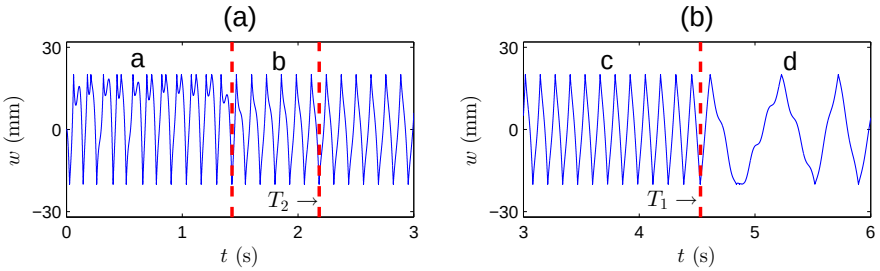

Figure 6: Four response regimes of VI NES: (a) three impacts per cycle; (b) two asymmetric impacts per cycle; (c) two symmetric impacts per cycle; (d) chaos with no duration of two impacts per cycle.

case performs better in terms of energy dissipation for the whole process.

Thus it can be concluded that tuning the cavity length of a VI NES to b_t is a feasible way of achieving a high TET efficiency under transient excitation. However, optimal efficiency of TET is achieved only in the stable branch of the SIM (between T_1 and T_2), which means that the VI NES is effective only in a certain range of the external forcing amplitude. For engineering applications, the cavity length of VI NES is usually fixed. To improve the robustness of VI NES for different types of excitation, tuning the clearances of multiple-degree-of-freedom VI NESs in parallel would be an alternative approach. For this, the optimal design of multiple VI-NESs is discussed in the next section.

4. Appropriate design of multiple VI-NESs

In this section, the academic model is updated by replacing single VI NES attachments with a parallel configuration of n VI NESs, and the dynamic system with $n = 2$ is illustrated schematically in Fig. 7. Dynamic motion is consequently related to a set of $n+1$ ordinary differential equations given by:

$$\begin{aligned} &M\ddot{x} + c_1\dot{x} + k_1 x = k_1 x_e + c_1 \dot{x_e} \\ &m\ddot{y}_1 = 0, \quad \forall |x - y_i| < b_1 \\ &m\ddot{y}_i = 0, \quad \forall |x - y_i| < b_i, \quad i = 2..n \end{aligned} \tag{38}$$

System (38) then can be rewritten in dimensionless form:

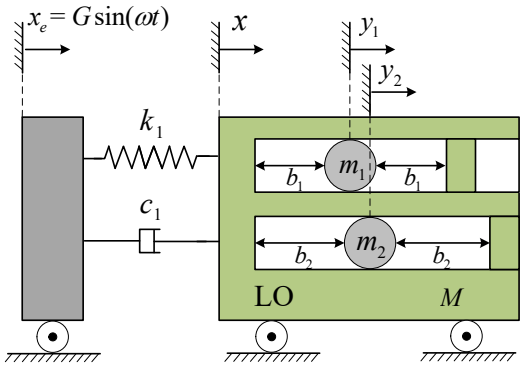

Figure 7: Schematic of the dynamic system: a harmonically excited LO coupled with two VI NESs in parallel

$$\begin{aligned}
&\ddot{X} + \varepsilon\lambda\dot{X} + X = \varepsilon F\sin\Omega\tau + \varepsilon^2\lambda F\Omega\cos\Omega\tau \\
&\varepsilon\ddot{Y}_1 = 0, \quad \forall |X-Y| < 1 \\
&\varepsilon\ddot{Y}_i = 0, \quad \forall |X-Y| < \Delta_i, \quad i = 2..n
\end{aligned} \tag{39}$$

where the variables of the displacements are dimensioned by $x = Xb_1$ and $y_i = Y_i b_1$. The new physical parameters are expressed as follows:

$$\begin{aligned}
&\varepsilon = \frac{m_1 + m_2 + ..m_n}{M}, \quad \alpha_i = \frac{m_i}{\varepsilon M}, \quad {\omega_0}^2 = \frac{k_1}{M}, \quad \tau = \omega_0 t, \\
&\lambda = \frac{c_1}{\varepsilon M\omega_0}, \quad \Omega = \frac{\omega}{\omega_0}, \quad F = \frac{G}{\varepsilon b_1}, \quad \Delta_i = \frac{b_i}{b_1}
\end{aligned} \tag{40}$$

In the same way, when $|X - Y_i| = \Delta_i$, an impact occurs. This yields:

$$\begin{aligned}
&X^+ = X^-, \quad {Y_i}^+ = {Y_i}^- \\
&\dot{X}^+ + \varepsilon\sum_{i=1}^{n}\alpha_i{\dot{Y}_i}^+ = \dot{X}^- + \varepsilon\sum_{i=1}^{n}\alpha_i{\dot{Y}_i}^- \\
&\dot{X}^+ - {\dot{Y}_i}^+ = -r\left(\dot{X}^- - {\dot{Y}_i}^-\right), \quad {\dot{Y}_j}^+ = {\dot{Y}_j}^-, \ (j \neq i)
\end{aligned} \tag{41}$$

Motions of the centre of mass and internal displacement are introduced in the following way:

$$V = X + \varepsilon\sum_{i=1}^{n}\alpha_i Y_i, \quad W_i = X - Y_i \tag{42}$$

Then, substituting Eq. (42) in Eqs. (41) and (40) gives

$$\begin{aligned}
&\ddot{V}+\varepsilon\lambda\frac{\dot{V}+\varepsilon\sum_{i=1}^{n}\dot{W}_i}{1+\varepsilon}+\frac{V+\varepsilon\sum_{i=1}^{n}W_i}{1+\varepsilon}=\varepsilon F\sin\Omega\tau\\
&\ddot{W}_i+\varepsilon\lambda\frac{\dot{V}+\varepsilon\sum_{i=1}^{n}\dot{W}_i}{1+\varepsilon}+\frac{V+\varepsilon\sum_{i=1}^{n}W_i}{1+\varepsilon}=\varepsilon F\sin\Omega\tau\\
&\forall|W_i|<\Delta_i
\end{aligned} \tag{43}$$

For this system, the impact condition (41) can be rewritten as:

$$\begin{aligned}
&V^+=V^-,\quad W_i^+=W_i^-,\quad \dot{V}^+=\dot{V}^-\\
&\text{if } |W_1|=1:\ \dot{W_1}^+=-r\dot{W_1}^-,\quad \dot{W}_i^+=\dot{W}_i^--\frac{\varepsilon\alpha_1(1+r)}{1+\varepsilon\alpha_1}\dot{W_1}^-,\ (i\neq 1)\\
&\text{if } |W_i|=\Delta_i:\ \dot{W_i}^+=-r\dot{W_i}^-,\quad \dot{W}_j^+=\dot{W}_j^--\frac{\varepsilon\alpha_i(1+r)}{1+\varepsilon\alpha_i}\dot{W_i}^-,\ (j\neq i)
\end{aligned} \tag{44}$$

Then multiple scales Eq. (12) and Eq. (13) are introduced in Eq. (44), system approximated at order ε^0 and order $\varepsilon^1$is obtained:

Order ε^0:

$$\begin{aligned}
&D_0^2V_0+V_0=0\\
&D_0^2W_{i0}+V_0=0,\quad \forall|W_{i0}|<\Delta_i
\end{aligned} \tag{45}$$

$$\begin{aligned}
&V_0^+=V_0^-,\quad W_0^+=W_0^-,\quad \text{for}|W_{i0}|=\Delta_i\\
&D_0V_0^+=D_0V_0^-,\quad D_0W_{i0}^+=-rD_0W_{i0}^-
\end{aligned} \tag{46}$$

Order ε^1:

$$\begin{aligned}
&D_0^2V_1+V_1=-2D_0D_1V_0-\lambda D_0V_0-\sum_{i=1}^{n}\alpha_iW_{i0}+V_0+F\sin(\tau_0+\sigma\tau_1)\\
&D_0^2W_i+V_1=-2D_0D_1V_0-\lambda D_0V_0-\sum_{i=1}^{n}\alpha_iW_{i0}+V_0+F\sin(\tau_0+\sigma\tau_1)\\
&\forall|W_{i0}|<1,\quad i=2..n
\end{aligned} \tag{47}$$

With the same method as used in Eq. (21), the SIM expression for multi VI NESs is finally deduced as:

$$
\begin{aligned}
A^2 &= (1-C_1)^2 + \frac{4C_1^2\Gamma^2}{\pi^2} \\
A^2 &= (\Delta_i - C_i)^2 + \frac{4C_i^2\Gamma^2}{\pi^2}, \quad i = 2..n
\end{aligned}
\tag{48}
$$

Here, it can be observed that each VI NES is dependent on the initial energy stored in the primary system and their performance is decoupled. With the principle of additivity and activities of VI NESs, the NESs efficiency is driven solely by the intrinsic properties of the LO and their own individual characteristics. Referring to the issue of optimal design for a single VI NES studied in section 3, it is fairly straightforward to extend the optimal criteria in the case of n-parallel VI NES by adjusting the two dimensionless variables Δ_i and α_i, so as to ensure the VI NESs are activated in a large band of excitation.

The transition point T_{i1}, which corresponds to the optimal activation energy of each VI NES that allows 1:1 TET, is given by:

$$
C_{i1} = \frac{\pi^2\Delta_i}{\pi^2 + 4\Gamma^2}, \quad A_{i1}^2 = \frac{4\Gamma^2\Delta_i^2}{\pi^2 + 4\Gamma^2}, \quad i = 2..n \tag{49}
$$

Thus the multiple VI NESs can be designed using the following rule: $A_{11}^2 < A_{21}^2 < ... < A_{n1}^2$. In this case, the activation energy of each VI NES is monotonously increased, making VI-NESs work robustly in different types of energy. Here, it is important to emphasize that SIM expressions in Eq. (48) are studied in the vicinity of the 1:1 resonance. If the anticipated motions of multiple VI NESs are not located in the vicinity of the 1:1 resonance, the principle of additivity may not be valid and the chaotic response may produce. In this case, the VI NES is not a NES in the sense that the transfer of energy is no longer irreversible, and the energy may spread back to the primary system, which will jeopardize the vibration mitigation performance. To restrict this situation, the energy threshold of each VI NES (i.e. the curve of each SIM stable branch projected on y axis) should not be set far away from each other, so that each VI NES can execute oscillation with identical frequency of LO. To analyze the chaotic characteristic of multiple VI NESs, Lyapunov exponent is an alternative way [27] and further study will be carried out on this aspect.

5. Experimental validation

The objective of this section is to experimentally verify the optimal design criteria proposed in the above sections. For periodic excitation, the focus is initially

to verify the periodic case at the resonance frequency and then to validate the results under a range of frequencies. As for transient excitation, the tuned method for optimal efficiency is verified, and two VI NESs in parallel are tested with the intention of improving robustness. The detailed procedures are as follows.

5.1. Periodic excitation

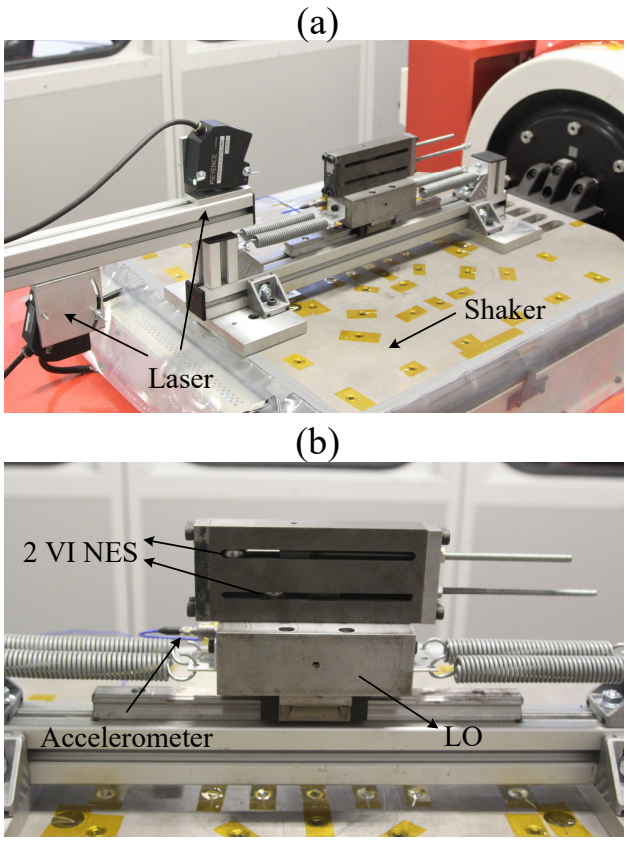

Figure 8: Experimental setup for periodic excitation:(a) global view of the configuration; (b) detailed view of the VI NES

The experimental setup of periodic excitation is presented in Fig. 8, where two clearances in parallel are used to decide whether one VI NES or two VI NESs are attached to the LO. The whole system was fixed to a 10 kN electrodynamic shaker. The raw signals were recorded using a digital oscilloscope and a bandpass filter

was applied to correct biases and suppress high frequency noise. The displacement of the LO as well as the imposed displacement of the shaker were measured by two contactless laser displacement sensors. The acceleration was measured by an accelerometer and the impacts between LO and VI NES could be judged from sudden changes of the acceleration of the LO. The parameters identified on the experimental setup and used for the calculation are given in Table. 2.

Table 2: Experimental parameters

Physical Parameters			
M	4.7 kg	c_1	3.02 Ns/m
k_1	1.147×10^4 N/m	m	32 g
Reduced Parameters			
ε	0.68 %	λ	1.91
f_0	7.86 Hz	r	0.6

With the variation of the clearance, three different responses of the LO under periodic excitation $G = 0.25$ mm were obtained, as shown in Fig. 9(a-c). Where the excitation frequency is fixed at the resonance frequency. As can be seen, the amplitude of the LO with $b = b_c$ was smaller than in the other two cases (i.e., steady state response with $b < b_c$ and chaotic SMR with $b > b_c$), since its fixed point was targeted at the transition point T_1. The optimal length of the cavity b_c under different types of excitation was calculated by Eq. (36) and is presented in Fig. 9(d). It can be observed that the experimental points are close to the theoretical values and located almost in a line. The differences between the theoretical and experimental values were mainly caused by the weakly nonlinear damping of the LO. Thus it can be demonstrated that the analytical calculation of b_c can be used to predict the efficient TET at resonance frequency for different types of excitation.

For the system in a range of frequencies, if the optimal clearance is still chosen by the value for resonance frequency, the responses of the other frequency points will not be optimal and may result in SMR or irregular response without any duration of two impacts per cycle. Therefore, there does not exist an optimal value of b for all frequencies. In [20], it is suggested that the objective of controlling the amplitude of the LO for a range of frequencies can be simplified to that of

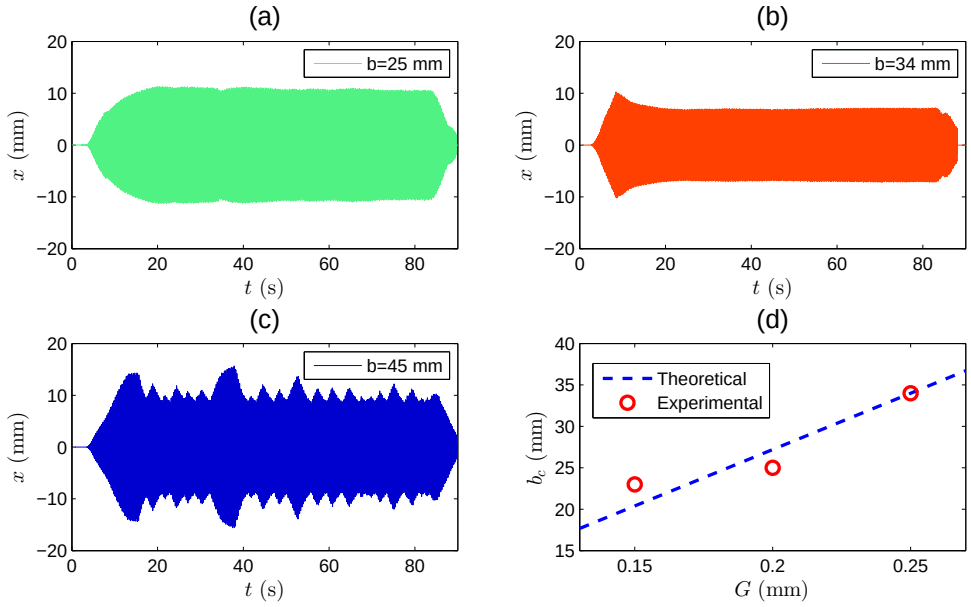

Figure 9: Experimental results of single VI NES: response of the LO under periodic excitation $G = 0.25$ mm with (a) $b = 25$ mm $(< b_c)$; (b) $b = 34$ mm $(= b_c)$; (c) $b = 45$ mm $(> b_c)$ and (d) optimal length of the cavity b_c under different types of excitation.

resonance frequency. Thus the clearance b_c is continually used as the optimal value.

Based on the sweep frequency test, frequency response functions (FRF) with $b < b_c$, $b = b_c$ and $b > b_c$ were obtained and are illustrated in Fig. 10(a). The detailed time-displacement responses are presented in Fig. 10(b-c). When $b < b_c$, the amplitude of LO is decreased with the addition of VI NES, and a small resonance peak still exists in this case. When $b > b_c$, the resonance peak has vanished and a large band of SMR can be found. However, the average amplitude of LO is still large in a range around the resonance frequency. When $b = b_c$, there exists a narrow range of frequency where SMR occurs. Although the VI NES cannot work at its optimal state for other frequencies except resonance frequency, the average amplitude of LO is smaller than the above two cases. Thus, the optimal design for a range of frequencies can directly use the analytical calculation of b_c, so as to make VI NES achieve a high TET efficiency for vibration mitigation.

For the above experimental configuration, the single VI NES case with the

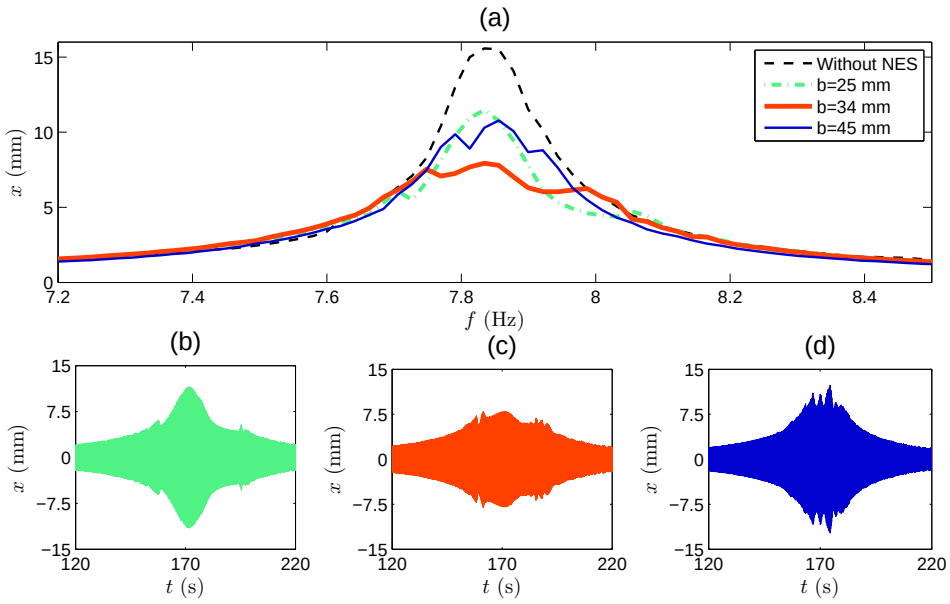

Figure 10: Experimental results of single VI NES: (a) frequency response curve of the LO with $G = 0.25$ mm and detailed view of response of the LO under sweep frequency test with (b) $b = 25$ mm ($< b_c$); (c) $b = 34$ mm ($= b_c$); (d) $b = 45$ mm ($> b_c$).

clearances $b = 34$ and 23 mm, was observed to be optimal for the excitation with $G = 0.25$ mm and 0.15 mm, respectively. Consequently, the clearances of two VI NESs in parallel were selected by these two values. The frequency response curves under $G = 0.25$ mm were recorded for different combinations of b_1 and b_2 and are showed in Fig. 11(a). The detailed time-displacement responses are presented in Fig. 11(b-c). When $b_1 = b_2 = 34$ mm, the amplitude of the LO around the resonance frequency is decreased. However, its maximum amplitude shifts to the left side and still has the same value (7.9 mm) as that of a single VI NES with $b = 34$ mm. When $b_1 = b_2 = 23$ mm, the amplitudes of the LO at the other frequencies are decreased. Yet a small resonance peak exists at the resonance frequency, since the clearance is not optimal for this excitation. When $b_1 = 23$ mm and $b_2 = 34$ mm, the small resonance peak has vanished and the frequency range for response with two impacts per cycle is increased. Although there is still a narrow range of frequencies where SMR occurs, its maximum amplitude of the LO has decreased to 4.9 mm. This value is far lower than in the two cases above, which means that adding two VI NESs with different clearance can perform a

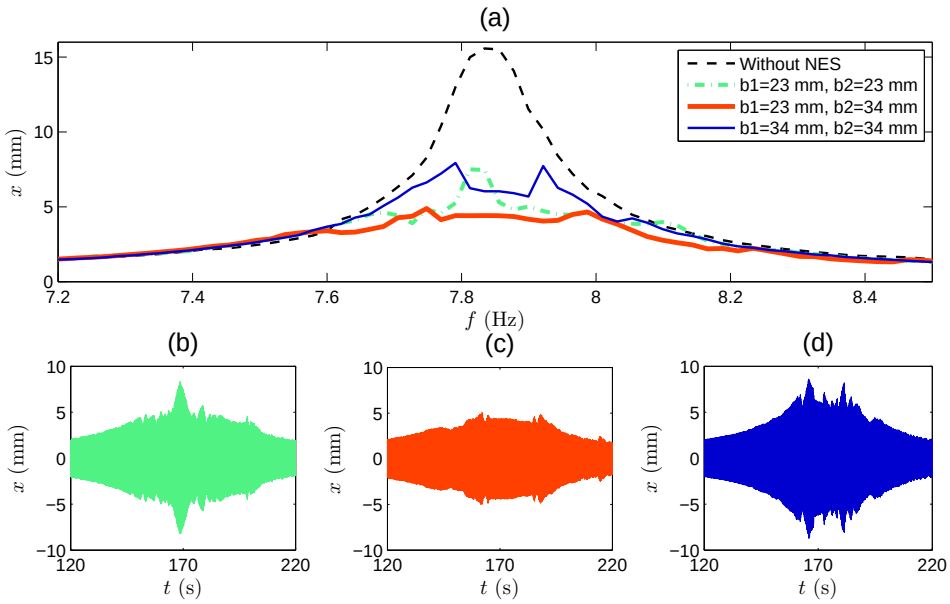

Figure 11: Experimental results of two VI NESs: (a) frequency response curve of the LO with $G = 0.25$ mm and detailed view of response of the LO under sweep frequency test with (b) $b_1 = 23$ mm, $b_2 = 23$ mm; (c) $b_1 = 23$ mm, $b_2 = 34$ mm; (d) $b_1 = 34$ mm, $b_2 = 34$ mm.

better TET efficiency and improve the robustness in a range of resonance frequencies.

Thus, the design criteria for optimally tuned VI NES can be summarized. If a single VI NES is applied, it is recommended that the clearance of VI NES should be optimized at the point of resonance frequency. By using the calculation of Eq. (36), the maximum amplitude of the LO can be controlled well at resonance condition (i.e., a single resonance frequency or a range of frequencies). In this case, a semi-active control method can also be used: by adjusting the clearance, a VI NES can be tuned to work robustly with its best performance. If multiple VI NESs are adopted to improve the robustness, the objective should first be to calculate the optimized clearance for the maximum excitation and then to choose a smaller length of clearance for a lower level of energy. By choosing VI NESs that are activated at different types of energy, a high TET efficiency can be obtained in a large band of excitation.

5.2. Transient excitation

The experimental setup for transient excitation is presented in Fig. 12, and the corresponding parameters can be found in Table 2. Here, the initial displacement of LO was obtained by stretching the string to a fixed position ($x_0 = 20\,\text{mm}$). Once the string was cut, both the LO and the VI NES started to vibrate, and the movement was recorded. The displacement and acceleration of the LO were measured by a laser and an accelerometer, respectively. By varying the length of cavity, the transition of response regimes was observed and the comparison of efficiency for different cavity lengths could be further studied.

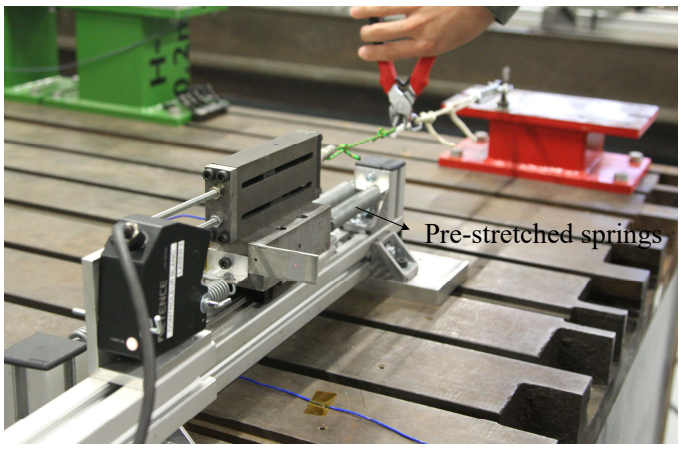

Figure 12: Experimental setup for transient excitation

The experimental results of single VI NES are presented in Fig. 13. As can be seen in Fig. 13(a), without VI NES, the vibration extinction of LO follows a natural exponential decrease; while with VI NES, it follows two phases of quasi-linear decrease, much faster than the exponential one, during which the displacement of LO decreases fast until it reaches a transition point (T_1) and the decay rate after this point is obviously lower than the previous one. An enlarged view of acceleration around this transition point is shown in Fig. 13(b). The sudden pulse of acceleration denotes an impact moment, and the transition between response regime of two symmetric impacts per cycle and chaos with an infinite number of impacts per cycle can be clearly identified.

Fig. 13(c) compares the displacement envelope of LO attached to a single VI NES with different cavity lengths. When $b = 10\,\text{mm} < b_t$, the master energy is higher than that of transition point T_2 (see Fig. 5), resulting in a relatively low

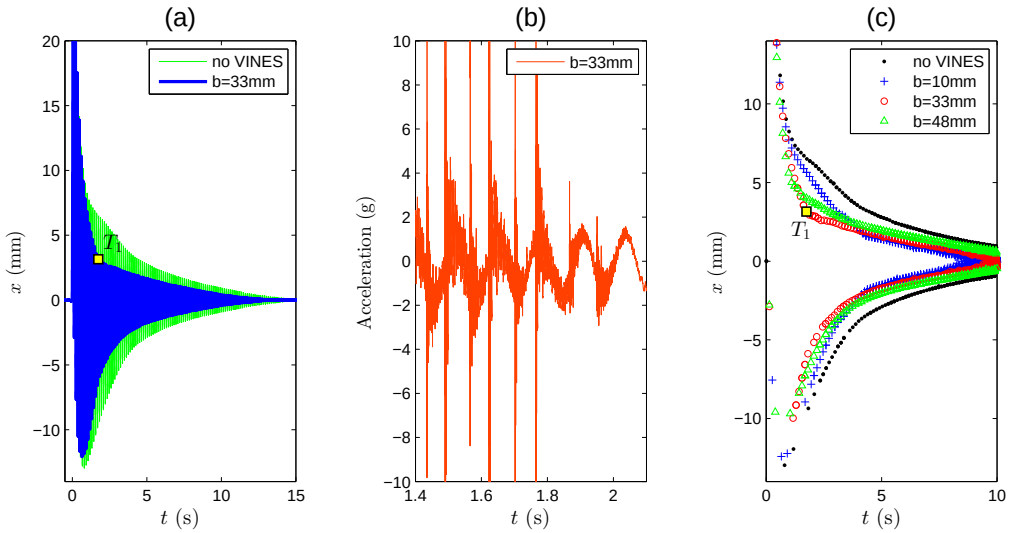

Figure 13: Experimental results of single VI NES: (a) time history of the displacement; (b) time history of the acceleration; (c) comparison of the displacement envelope with different b.

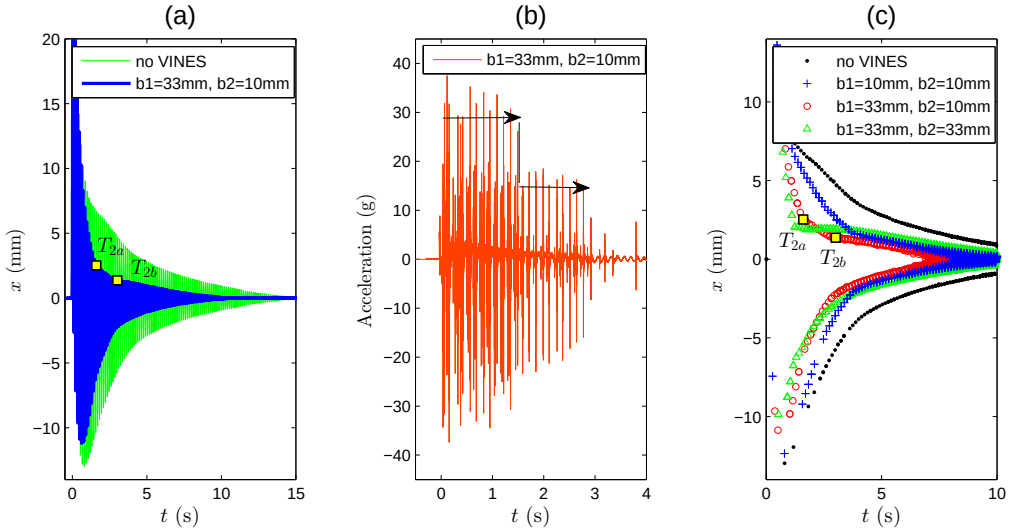

Figure 14: Experimental results of two VI NESs: (a) time history of the displacement; (b) time history of the acceleration; (c) comparison of the displacement envelope with different b.

decay rate. When $b = 33\,\text{mm} = b_t$ and $b = 48\,\text{mm} > b_t$, both their responses start from a regime with two symmetric impacts per cycle, causing the vibration extinction of LO to directly follow a quasi-linear decrease. In addition, it can be observed that the transition point T_1 with $b = b_t$ is lower than that with $b > b_t$. Thus, tuning the cavity length to b_t is a feasible way of obtaining an optimal TET efficiency during the whole vibration process.

The experimental results for two VI NESs are presented in Fig. 14. When the cavity lengths of two VI NESs are set at two different values with $b_1 = 33\,\text{mm}$ and $b_2 = 10\,\text{mm}$, the vibration extinction of LO follows three quasi-linear decreases (see Fig. 14(a)). If the amplitude of LO is higher than the transition point T_1a, the first VI NES with a large cavity length is activated with two impacts per cycle. If the amplitude of LO is located in the range between T_{1a} and T_{1b}, the first VI NES escapes from the activation and the second VI NES with a small clearance is activated with 1:1 resonance capture. The principle of separate activation can also be found from the time history of the acceleration (see Fig. 14(b)). As can be seen, the impact strength of VI NES is related to the cavity length. The horizontal arrows show the two activations of two VI NESs with different cavity lengths, and the vertical line illustrates the sudden change between them.

Fig. 14(c) shows the comparison of the displacement envelope of LO attached to two VI NESs with different cavity lengths. With the addition of another ball, the three groups of two VI NESs perform better than the case of single VI NES. When $b_1 = b_2 = 10\,\text{mm}$, the decay rate of first decrease phase is slightly improved, while the displacement of the transition point is almost the same as that of a single VI NES with $b = 10\,\text{mm}$. When $b_1 = b_2 = 33\,\text{mm}$, the decay rate of first decrease phase is optimal. However, the efficiency at low energy level is not improved, and the decay rate is far lower than the other two cases. When $b_1 = 33\,\text{mm}$ and $b_2 = 10\,\text{mm}$, the decay rate of first decrease phase is close to that of VI NESs with $b_1 = b_2 = 33\,\text{mm}$. At low energy level (the amplitude of LO is lower than T_{1a}), the decay rate becomes better than in the other two cases. Thus this group of VI NESs can work robustly and efficiently for different kinds of transient excitation.

In summary, the tuned method for transient excitation is verified. The analytical calculation of Eq. (37) is demonstrated to predict the optimal clearance well. Moreover, the principles of additivity and separate activities of multiple VI NESs are observed, and the robustness of vibration control can be improved for a large band of transient excitation.

6. Conclusion

The ultimate goal of this paper is to propose the design criteria for optimally tuned Vibor-Impact (VI) NES to control the vibration under periodic and transient excitation. To this end, a generalized dimensionless model of a 2-degrees-of-freedom system comprising a harmonically excited LO strongly coupled to a VI NES is studied. An analytically obtained Slow Invariant Manifold (SIM) is used to explain the different response regimes. The transition point (i.e., T_1) between the regime with two symmetrical impacts per cycles and that of Strongly Modulated Response (SMR) is demonstrated to be optimal for periodic excitation. Then, a bifurcation analysis is carried out. An activation energy threshold for targeted energy transfer is obtained and used to design an optimal criterion for a single NES.

For transient excitation, the critical point (i.e., T_2) between the regime with two symmetrical impacts per cycles and two asymmetrical impacts per cycles is adopted to calculate the optimal clearance, and it proves that tuning the initial master energy at this point can achieve a high TET efficiency during the whole vibration process. Thirdly, the procedure is extended to the case of multiple VI NESs in parallel. Two principles of additivity and separate activities of VI NESs are verified theoretically and experimentally.

Finally, experiments involving the whole system for periodic and transient excitation are performed. The results show that the analytical calculation of the clearance can not only predict the efficient TET at resonance frequency, but can also achieve an optimal performance to protect the primary system in a range of frequencies. Furthermore, the design criteria for a single VI NES can be straightforward for the application of multiple VI NESs, so as to make VI NES work robustly under different types of excitation.

References

[1] P. Lieber, D. Jensen, An acceleration damper: development, design and some applications, Trans. ASME 67 (10) (1945) 523–530.

[2] R. A. Ibrahim, Vibro-impact dynamics: modeling, mapping and applications, Vol. 43, Springer Science & Business Media, Berlin, 2009.

[3] V. I. Babitsky, Theory of vibro-impact systems and applications, Springer Science & Business Media, Berlin, 2013.

[4] A. Afsharfard, Suppressing forced vibrations of structures using smart vibro-impact systems, Nonlinear Dynamics 83 (3) (2016) 1643–1652.

[5] M. Dimentberg, D. Iourtchenko, Random vibrations with impacts: a review, Nonlinear Dynamics 36 (2) (2004) 229–254.

[6] A. Afsharfard, A. Farshidianfar, Free vibration analysis of nonlinear resilient impact dampers, Nonlinear Dynamics 73 (1-2) (2013) 155–166.

[7] D.-G. Zhang, J. Angeles, Impact dynamics of flexible-joint robots, Computers & structures 83 (1) (2005) 25–33.

[8] Y. Lee, A. F. Vakakis, L. Bergman, D. McFarland, G. Kerschen, F. Nucera, S. Tsakirtzis, P. Panagopoulos, Passive non-linear targeted energy transfer and its applications to vibration absorption: a review, Proceedings of the Institution of Mechanical Engineers, Part K: Journal of Multi-body Dynamics 222 (2) (2008) 77–134.

[9] A. F. Vakakis, O. Gendelman, L. Bergman, D. McFarland, G. Kerschen, Y. Lee, Nonlinear targeted energy transfer in mechanical and structural systems, Vol. 156, Springer Science & Business Media, Berlin, 2008.

[10] F. Nucera, A. Vakakis, D. McFarland, L. Bergman, G. Kerschen, Targeted energy transfers in vibro-impact oscillators for seismic mitigation, Nonlinear Dynamics 50 (3) (2007) 651–677.

[11] F. Nucera, F. Lo Iacono, D. McFarland, L. Bergman, A. Vakakis, Application of broadband nonlinear targeted energy transfers for seismic mitigation of a shear frame: Experimental results, Journal of Sound and Vibration 313 (1) (2008) 57–76.

[12] I. Karayannis, A. Vakakis, F. Georgiades, Vibro-impact attachments as shock absorbers, Proceedings of the Institution of Mechanical Engineers, Part C: Journal of Mechanical Engineering Science 222 (10) (2008) 1899–1908.

[13] Y. Lee, F. Nucera, A. Vakakis, D. McFarland, L. Bergman, Periodic orbits, damped transitions and targeted energy transfers in oscillators with vibro-impact attachments, Physica D: Nonlinear Phenomena 238 (18) (2009) 1868–1896.

[14] O. Gendelman, Analytic treatment of a system with a vibro-impact nonlinear energy sink, Journal of Sound and Vibration 331 (2012) 4599–4608.

[15] E. Gourc, S. Seguy, G. Michon, A. Berlioz, B. Mann, Quenching chatter instability in turning process with a vibro-impact nonlinear energy sink, Journal of Sound and Vibration 355 (2015) 392–406.

[16] O. Gendelman, A. Alloni, Dynamics of forced system with vibro-impact energy sink, Journal of Sound and Vibration 358 (2015) 301–314.

[17] T. Li, S. Seguy, A. Berlioz, On the dynamics around targeted energy transfer for vibro-impact nonlinear energy sink, Nonlinear Dynamics 87 (3) (2017) 1453–1466.

[18] T. Li, D. Qiu, S. Seguy, A. Berlioz, Activation characteristic of a vibro-impact energy sink and its application to chatter control in turning, Journal of Sound and Vibration 405 (2017) 1 – 18.

[19] R. Viguié, G. Kerschen, Nonlinear vibration absorber coupled to a nonlinear primary system: a tuning methodology, Journal of Sound and Vibration 326 (3) (2009) 780–793.

[20] T. Li, S. Seguy, A. Berlioz, Optimization mechanism of targeted energy transfer with vibro-impact energy sink under periodic and transient excitation, Nonlinear Dynamics 87 (4) (2017) 2415–2433.

[21] T. A. Nguyen, S. Pernot, Design criteria for optimally tuned nonlinear energy sinks—part 1: transient regime, Nonlinear Dynamics 69 (1) (2012) 1–19.

[22] T. Li, E. Gourc, S. Seguy, A. Berlioz, Dynamics of two vibro-impact nonlinear energy sinks in parallel under periodic and transient excitations, International Journal of Non-Linear Mechanics 90 (2017) 100 – 110.

[23] E. Boroson, SamyMissoum, P.-O. Mattei, C. Vergez, Optimization under uncertainty of parallel nonlinear energy sinks, Journal of Sound and Vibration 394 (2017) 451 – 464.

[24] B. Vaurigaud, A. T. Savadkoohi, C.-H. Lamarque, Targeted energy transfer with parallel nonlinear energy sinks. part i: Design theory and numerical results, Nonlinear dynamics 66 (4) (2011) 763–780.

[25] E. Gourc, G. Michon, S. Seguy, A. Berlioz, Targeted energy transfer under harmonic forcing with a vibro-impact nonlinear energy sink: Analytical and experimental developments, Journal of Vibration and Acoustics 137 (3) (2015) 031–008.

[26] V. Pilipchuk, Closed-form solutions for oscillators with inelastic impacts, Journal of Sound and Vibration 359 (2015) 154–167.

[27] T. Li, C.-H. Lamarque, S. Seguy, A. Berlioz, Chaotic characteristic of a linear oscillator coupled with vibro-impact nonlinear energy sink, Nonlinear Dynamics 91 (4) (2018) 2319–2330.